



Cite this: *Phys. Chem. Chem. Phys.*,
2019, 21, 5232

Towards high-level theoretical studies of large biodiesel molecules: an ONIOM/RRKM/Master-equation approach to the isomerization and dissociation kinetics of methyl decanoate radicals†

Qinghui Meng,^{a,b} Yicheng Chi,^a Lidong Zhang, ^{a,b} Peng Zhang^{*a} and Liusi Sheng^b

The isomerization and dissociation reactions of methyl decanoate (MD) radicals were theoretically investigated by using high-level theoretical calculations based on a two-layer ONIOM method, employing the QCISD(T)/CBS method for the high layer and the M06-2X/6-311++G(d,p) method for the low layer. Temperature- and pressure-dependent rate coefficients for the involved reactions were computed by using the transition state theory and the Rice–Ramsperger–Kassel–Marcus/Master-equation method. The structure–reactivity relationships were explored for the complicated multiple-well interconnected system of ten isomeric MD radicals. Comparative studies of methyl butanoate (MB) and MD were also performed systematically. Results show that the isomerization reactions are appreciably responsible for the population distribution of MD radicals at low and intermediate temperatures, while the β -scission reactions are dominant at higher temperatures. Although the rate constants of MB specific to methyl esters are close to those of MD in certain temperature ranges, MB is unable to simulate most of the dissociation reactions due to its short aliphatic chain. Significant differences of rate constants for isomerization reactions were observed between the calculated results and the literature data, which were estimated by analogy to alkane systems, but the rate constants of β -scissions show generally good agreement between theory and experiment. The current work extends kinetic data for isomerization and dissociation reactions of MD radicals, and it serves as a reference for the studies of detailed combustion chemistry of practical biodiesels.

Received 4th September 2018,
Accepted 5th February 2019

DOI: 10.1039/c8cp05593a

rsc.li/pccp

1. Introduction

Biodiesel is regarded as one of the most promising fuel alternatives due to its renewable and various feedstocks, environmental benefits, and attractive physicochemical properties.^{1–3} It is primarily composed of long-carbon-chain (12–20 carbon atoms) saturated and unsaturated monoesters derived from chemically reacting lipids with an alcohol through transesterification reactions.⁴ Compared with biodiesels obtained from animal oils, those from vegetable oils mainly consist of saturated fatty acid methyl or ethyl esters. Biodiesels can be used in pure

form or in blends with petroleum diesel at any concentration in most injection pump diesel engines.^{1,5} Although knowledge about biodiesel combustion characteristics is essential for its applications, only a few combustion chemistry modeling works (specifically on developing detailed reaction mechanisms and their applications to simulating typical combustion parameters) have been done to investigate the combustion of practical biodiesels.^{6–9}

Methyl decanoate [MD, $\text{CH}_3(\text{CH}_2)_8\text{COOCH}_3$], the largest component (65% by mass) in cuphea biodiesel,¹⁰ has been proposed as a typical biodiesel surrogate. Its desirable fuel properties (*e.g.* low vapor pressure and melting point) make it experimentally accessible to traditional techniques. Herbinet *et al.*¹¹ developed a detailed reaction mechanism (aka detailed kinetic model) of MD based on the reaction mechanisms of *n*-heptane,¹² iso-octane,¹³ and methyl butanoate [MB, $\text{CH}_3(\text{CH}_2)_2\text{COOCH}_3$]¹⁴ and by combining specific oxidation properties of methyl esters. Subsequently, Herbinet *et al.*¹⁵ updated the MD mechanism by adding the sub-mechanisms of methyl 5-decanoate and methyl

^a Department of Mechanical Engineering, The Hong Kong Polytechnic University, Hung Hom, Kowloon, Hong Kong. E-mail: pengzhang.zhang@polyu.edu.hk; Fax: +852 23654703; Tel: +852 27666664

^b National Synchrotron Radiation Laboratory, University of Science and Technology of China, Hefei, Anhui 230029, P. R. China. E-mail: zld@ustc.edu.cn; Fax: +86 551 65141078; Tel: +86 551 63607923

† Electronic supplementary information (ESI) available. See DOI: 10.1039/c8cp05593a

9-decanoate and used it to explore the combustion of biodiesels in a jet-stirred reactor. Glaude *et al.*¹⁶ developed a detailed reaction mechanism for esters up to MD based on the EXGAS code for automatically generating reaction mechanisms. It should be noted that the rate constants of recombination and dissociation reactions in these mechanisms were either calculated by analogy to alkanes or derived from the quantitative structure-reactivity relationships.¹⁶ In addition, the rate constants of H-abstraction reactions used in these mechanisms were evaluated by using the Evans-Polanyi correlation for hydrocarbons.¹⁶ It was found that the overestimated rate constants resulted in faster reaction rates by about a factor of two at 1000 K.¹⁶ As pointed out by Diévert *et al.*,¹⁷ different prescriptions of rate constants for the reactions involving molecules with the ester functional group result in appreciably different MD oxidation pathways and model predictions to global combustion parameters. Thus, it is essential and urgent to obtain more reliable rate constants of MD reaction systems.

Recent advances in theoretical and computational chemistry enable the accurate evaluation of thermal and kinetic parameters of relatively small molecules. It is known that extrapolation to the coupled cluster single and double excitation and perturbative triples CCSD(T)/complete basis set(CBS) predicts energy barriers with uncertainties of less than 1.1 kcal mol⁻¹,¹⁸ and that the extrapolation of quadratic configuration interaction with singles, doubles and perturbative inclusion of triples QCISD(T)/CBS with a sequence of the correlation-consistent, polarized-valence, triple- ζ (cc-pVTZ), and quadruple- ζ (cc-pVQZ) basis sets can evaluate energy barriers with uncertainties of around 1.0 kcal mol⁻¹.¹⁹ Therefore, high-level theoretical studies aiming to understand the chemical kinetics of realistic biodiesels have been focused on small surrogate molecules.^{20–22} However, Diévert *et al.*¹⁷ indicated that small methyl esters such as MB are not ideal surrogates to simulate real biodiesel. More recently, Pyl *et al.*²³ performed the pyrolysis of MD in a bench-scale reactor equipped with a dedicated on-line analysis section with temperature varied from 873 K to 1123 K and at a fixed pressure of 1.7 bar. They found that MD was largely consumed by H-abstraction reactions, implying that the unimolecular dissociation and the isomerization reactions of MD radicals may become increasingly important at high temperatures.

Despite the importance of the isomerization and the dissociation reactions of biodiesel radicals, only a few studies have been conducted on their theoretical chemical kinetics. The composite method CBS-QB3 was employed by Glaude *et al.*¹⁶ for energy predictions of some β -scission reactions of small methyl esters, which have an average deviation of ± 1.0 kcal mol⁻¹. For biodiesel surrogate molecules with more than 10 heavy atoms, energy calculations with the aforementioned high-level methods are formidable due to their intensive computational load. To meet this challenge, a two-layer ONIOM method was developed by Zhang *et al.*,^{24,25} aiming to directly calculate the accurate thermochemical and chemical kinetic parameters of practical biodiesel constituents. The method was systematically validated for the H-abstraction reactions of saturated esters

$C_nH_{2n+1}COOC_mH_{2m+1}$ ($n = 1–5, 9, 15; m = 1, 2$) and unsaturated esters $C_nH_{2n-1}COOCH_3$ ($n = 2–5, 17$) by hydrogen radicals. The predictions for energy barriers and heats of reaction have comparable accuracy to the QCISD(T)/CBS method with deviations being less than 0.15 kcal mol⁻¹.

In the present work, the rate constants of the isomerization and dissociation reactions were theoretically investigated for all MD radicals. Density functional theory (DFT) was employed to locate the stationary points on the potential energy surface. Single-point energies of all the species considered herein were refined with the two-layer ONIOM method of Zhang *et al.*²⁴ Rate constants were then computed with the TST-RRKM theory at temperatures from 500 K to 2500 K and at the pressures of 0.1, 1, 10 and 100 atm. Moreover, a comparative study of the MD radicals herein with the previous studies on MD radicals¹¹ and MB radicals²⁰ was conducted by analyzing the corresponding thermal and kinetic data.

2. Theoretical methodology

2.1 Potential energy surfaces

The geometry optimizations, vibrational frequencies, and zero-point energies for all of the stationary points on the potential energy surface (PES) of MD radicals were obtained at the M06-2X/6-311++G(d,p) level of theory. The transition states corresponding to desired reaction coordinates were identified by using imaginary frequency analysis and visual inspection. For those ambiguous cases, intrinsic reaction path analysis was utilized to examine the connections of each saddle point to its local minima. All harmonic frequencies used herein are the original data from the density functional theory calculations without using scaling factors.²¹

The higher-level single-point energies were calculated by using a two-layer ONIOM method,²⁴ employing QCISD(T)/CBS for the high layer and the M06-2X-favor DFT method for the low layer. The present ONIOM method predicts the high-level energy of the entire system by its low-level energy plus the correction from the difference between the high-level and low-level energies of the chemically active portion (CAP), given by

$$E^{\text{ONIOM}}[\text{High:Low}] = E^{\text{Low}}(\text{R}) + E^{\text{High}}(\text{CAP}) - E^{\text{Low}}(\text{CAP}) \quad (\text{E1})$$

For the isomerization and dissociation reactions of MD radicals, the CAP consists of the active site and two neighboring CH₂ (or CH₃, COO) groups on the one side and two neighboring CH₂ (or CH₃, COO) groups on the other side. The ONIOM [QCISD(T)/CBS:DFT] energy is calculated by

$$E^{\text{ONIOM}}[\text{QCISD(T)CBS:DFT}] = E^{\text{ONIOM}}[\text{QCISD(T)/CBS:DFT}]_{\text{DZ} \rightarrow \text{TZ}} + \{E^{\text{ONIOM}}[\text{MP2/CBS:DFT}]_{\text{DZ} \rightarrow \text{TZ}} - E^{\text{ONIOM}}[\text{MP2/CBS:DFT}]_{\text{DZ} \rightarrow \text{TZ}}\} \quad (\text{E2})$$

where,

$$\begin{aligned} E^{\text{ONIOM}}[\text{QCISD(T)CBS:DFT}]_{\text{DZ} \rightarrow \text{TZ}} &= E^{\text{ONIOM}}[\text{QCISD(T)/TZ:DFT}] \\ &+ \{E^{\text{ONIOM}}[\text{QCISD(T)/TZ:DFT}] - E^{\text{ONIOM}}[\text{QCISD(T)/DZ:DFT}] \\ &\times 0.4629\} \end{aligned} \quad (\text{E3})$$

$$E^{\text{ONIOM}}[\text{MP2/CBS:DFT}]_{\text{DZ} \rightarrow \text{TZ}} = E^{\text{ONIOM}}[\text{MP2/DZ:DFT}] + \{E^{\text{ONIOM}}[\text{MP2/DZ:DFT}] - E^{\text{ONIOM}}[\text{MP2/TZ:DFT}] \times 0.6938\} \quad (\text{E4})$$

$$E^{\text{ONIOM}}[\text{MP2/CBS:DFT}]_{\text{DZ} \rightarrow \text{TZ}} = E^{\text{ONIOM}}[\text{MP2/TZ:DFT}] + \{E^{\text{ONIOM}}[\text{MP2/TZ:DFT}] - E^{\text{ONIOM}}[\text{MP2/DZ:DFT}] \times 0.4629\} \quad (\text{E5})$$

The ONIOM [QCISD(T)/CBS:DFT] method has been systematically validated in the previous theoretical studies on the H-abstraction reactions of saturated and unsaturated alkyl esters by hydrogen radicals, and its reliability has been confirmed through comparisons with the QCISD(T)/CBS results with deviations being less than 0.15 kcal mol⁻¹.^{24,25} More details of the ONIOM method can be found in the literature.^{24,25} All the present calculations were performed by using the Gaussian 09 program.²⁶

2.2 Temperature- and pressure-dependent kinetics

For the reactions with well-pronounced transition states, the transition state theory (TST) was used for the calculation of rate constants, where the rigid rotor harmonic oscillator (RRHO) assumption was employed for all the internal degrees of freedom except for those low-frequency torsional modes. For each torsional mode, the hindrance potentials as a function of the torsional angle were explicitly obtained at the M06-2X/6-311++G(d,p) level *via* relaxed potential energy surface scans with an increment angle of 12°. For the reactions involving the transfer of hydrogen atoms, the tunneling effect on the rate constants was routinely taken into account on the basis of the asymmetric Eckart model.²⁷

As will be shown shortly in Section 3, the PES of the isomerization and dissociation reactions of MD radicals consists of multiple interconnected potential wells and multiple product channels. Pressure dependence was calculated by using multiple-well Master equation analysis with a single-exponential-down model, $\Delta E_{\text{down}} = 200(T/300)^{0.85}$ cm⁻¹, to approximate the collisional energy transfer probability. This model has been validated in relevant studies of MB²¹ and *n*-butyl.²⁸ The Lennard-Jones (L-J) parameters for MD were approximated by $\sigma = 7.3$ Å and $\varepsilon = 604.7$ cm⁻¹, which were utilized in the MD system previously.²⁹ For the Ar bath gas, the L-J parameters $\sigma = 3.47$ Å and $\varepsilon = 78.89$ cm⁻¹ were recommended by Hippler *et al.*³⁰ Phenomenological rate coefficients were obtained by solving time-dependent RRKM-based master equations³¹ implemented in the MESS computer program.³¹

3. Results and discussion

3.1 Potential energy surfaces

3.1.1 Representative PESs of MD radicals. The PESs for the isomerization and decomposition reactions of MD radicals were constructed and investigated systematically herein. Ten isomeric MD radicals can either undergo isomerization reactions or decompose to smaller compounds *via* β-scission reactions. Moreover, the isomerization and β-scission reactions of another isomer, $\text{CH}_3(\text{CH}_2)_6\text{CHCH}=\text{C(OH)OCH}_3$, were also explored (see Fig. S1 in the ESI†). The complete PES consisting

of multiple, interconnected species wells and multiple product channels is extremely complicated because of the large number of isomerization reactions between all the potential wells. For clarity and simplicity, the PES for each isomer was presented separately by only showing the reaction pathways directly connected to it. The energies of the stationary points on the PESs were determined at the ONIOM[QCISD(T)/CBS:DFT]/M06-2X/6-311++G(d,p) level and listed in Table S1 in the ESI.†

The nomenclature of these ten different radicals is consistent with that used in the previous study.¹⁴ To be specific, the radicals $\text{CH}_3(\text{CH}_2)_7\text{CHCOOCH}_3$, $\text{CH}_3(\text{CH}_2)_6\text{CHCH}_2\text{COOCH}_3$, $\text{CH}_3(\text{CH}_2)_5\text{CH}(\text{CH}_2)_2\text{COOCH}_3$, $\text{CH}_3(\text{CH}_2)_4\text{CH}(\text{CH}_2)_3\text{COOCH}_3$, $\text{CH}_3(\text{CH}_2)_3\text{CH}(\text{CH}_2)_4\text{COOCH}_3$, $\text{CH}_3(\text{CH}_2)_2\text{CH}(\text{CH}_2)_5\text{COOCH}_3$, $\text{CH}_3\text{CH}_2\text{CH}(\text{CH}_2)_6\text{COOCH}_3$, $\text{CH}_3\text{CH}(\text{CH}_2)_7\text{COOCH}_3$, $\text{CH}_2(\text{CH}_2)_8\text{COOCH}_3$ and $\text{CH}_3(\text{CH}_2)_8\text{COOCH}_2$ are denoted by MD2J, MD3J, MD4J, MD5J, MD6J, MD7J, MD8J, MD9J, MD10J and MDMJ, respectively. The isomer $\text{CH}_3(\text{CH}_2)_6\text{CHCH}=\text{C(OH)OCH}_3$ is denoted by R11.

The PES for MD2J is displayed in Fig. 1, where the β-scission reaction forming *n*-heptane radical and methyl acrylate (*i.e.* P1) was chosen as the entrance channel. The other β-scission reaction leading to $\text{CH}_3(\text{CH}_2)_7\text{CH}=\text{C}=\text{O}$ and CH_3O has a very high energy barrier compared with the other reactions on the PES and therefore is not shown for clearer illustration. For all the reaction channels on this and the subsequent PESs, the energies are relative to that of MD2J, which was chosen as a reference and defined as zero. As shown in Fig. 1, MD2J can isomerize to MD3J, MD4J, ..., MD10J, and MDMJ *via* hydrogen migration reactions with energy barriers ranging from 17.1 kcal mol⁻¹ to 39.2 kcal mol⁻¹. MD2J can isomerize to R11 because of the conjugation effect as a result of the overlap of p-orbitals of the radical site with the adjacent π-bond of the carbonyl group. However, the energy barrier of the isomerization reaction is as high as 42.1 kcal mol⁻¹ due to the strong steric effect.

The strain energy and the steric effect have a critical influence on the energy barrier for the isomerization reactions. When the number of atoms of the transition state ring is larger than 6, the strain energy of the ring remains nearly unchanged,

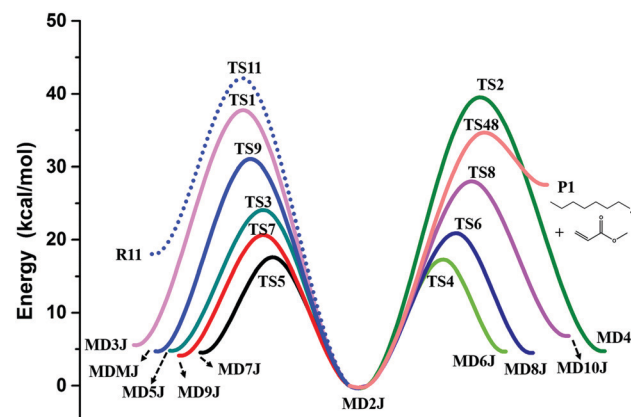


Fig. 1 Potential energy surface for the isomerization and β-scission reactions of MD2J at the ONIOM [QCISD(T)/CBS:DFT]/M06-2X/6-311++G(d,p) level.

and thus the energy barrier is determined by the steric effect. The steric effect is stronger for the transition state ring (such as TS2, TS4, TS6, and TS8) with an even number of atoms than that (such as TS1, TS3, TS5, and TS7) with an odd number of atoms. As shown in Fig. 1, the energy barriers of the isomerization reactions from MD2J to MD3J, MD4J, MD5J, MD6J, MD7J, MD8J, MD9J, MD10J and MDMJ are 37.7 kcal mol⁻¹ (TS1), 39.2 kcal mol⁻¹ (TS2), 23.9 kcal mol⁻¹ (TS3), 17.1 kcal mol⁻¹ (TS4), 17.6 kcal mol⁻¹ (TS5), 20.7 kcal mol⁻¹ (TS6), 20.6 kcal mol⁻¹ (TS7), 28.0 kcal mol⁻¹ (TS8), and 31.0 kcal mol⁻¹ (TS9), respectively. It can be seen that the reaction of MD2J → MD6J (*via* TS4) through a 6-centered ring transition state is the most energetically favorable one with the lowest energy barrier, 17.1 kcal mol⁻¹. The reaction of MD2J → MD7J through a 7-centered ring transition state (TS5) has an increased energy barrier of 17.6 kcal mol⁻¹. In comparison with the corresponding alkyl radicals,³² the MD radicals also show a non-monotonic trend due to the reduction of symmetry with the existence of ester moieties.

For the reaction without the ester functionality in the transition state ring, the energy barrier decreases and then increases as the size of the transition state ring increases. This is because the ester functional moieties will strengthen the steric effect if they are not included in the transition state ring. This is also observed in other MD radicals, such as MD3J, whose PES is shown in Fig. 2. The downturn of the energy barrier is attributed to the lower strain energy with increasing size of the transition state ring, and the uptrend is caused by a stronger steric effect with increasing size of the transition state ring, as discussed above.

The PES of MD3J is shown in Fig. 2, where two important dissociation reactions are the β -scission reactions forming $\text{CH}_3(\text{CH}_2)_6 + \text{CH}_2=\text{CHCH}_2\text{C}(=\text{O})\text{CH}_3$ (*via* TS50) and $\text{CH}_3(\text{CH}_2)_6\text{CH}=\text{CH}_2 + \text{C}(=\text{O})\text{OCH}_3$ (*via* TS51) with the transition state energy barrier of 30.0 kcal mol⁻¹ and 30.6 kcal mol⁻¹, respectively. It is found that the isomerization reaction of MD3J → MD8J has the lowest transition state (TS15) energy of 19.4 kcal mol⁻¹, which is significantly lower than those of the two β -scission reactions. However, the reaction of MD3J → MD8J

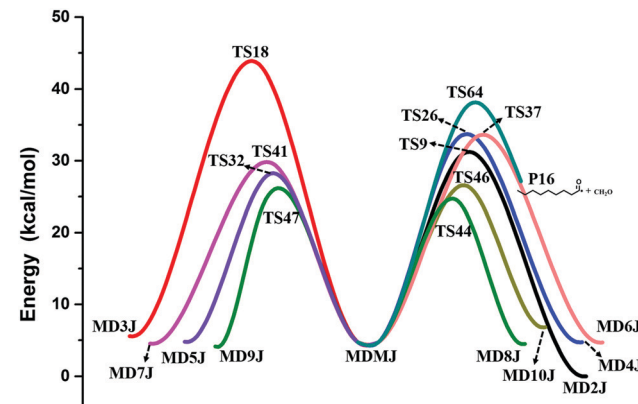


Fig. 3 Potential energy surface for the isomerization and β -scission reactions of MDMJ at the ONIOM [QCISD(T)/CBS:DFT]//M06-2X/6-311++G(d,p) level.

is expected to be kinetically unfavorable unless the temperature is sufficiently low because TS15 has a tight, 7-membered ring structure. Similar trends have also been confirmed for other MD radicals such as MD4J, ..., and MD10.

The PES of MDMJ is shown in Fig. 3. For the reactions involving MDMJ, the transition state ring contains the ester functionality, and the energy barrier decreases with increasing size of the transition state ring. This is because the strain energy increases with the inclusion of ester functionality in the transition state ring. The isomerization reaction from MDMJ to MD9J (*via* TS47) has the second lowest transition state energy, 24.8 kcal mol⁻¹, which can compete with MDMJ → MD8J (*via* TS44) with the lowest transition state energy of 24.4 kcal mol⁻¹ at low temperatures. As temperature increases, the dominant channel for MDMJ is the β -scission reaction producing P16 *via* a much looser transition state (TS64) than those of the isomerization reactions. All the relative energies and energy barriers of transition states for all isomerization reactions connecting the ten MD radicals are listed in Table S2 in the ESI.[†]

3.1.2 Discussion on energies of MD radicals. As mentioned in the Introduction, the previous reaction mechanisms of MD were mainly developed from analogy to alkanes and MB due to the scarcity of theoretical kinetic data for large esters.¹¹ In fact, the activation energies of isomerization reactions of MD radicals were estimated by the sum of the activation energy of the corresponding H-abstraction and the strain energy of the transition state ring in the isomerization.^{11,12} Although the effect of the ester functionality on the activation energy of the H-abstraction reaction forming MD2J has been estimated, the deviations of activation energy for the H-abstraction reactions forming other MD radicals are larger than 2.0 kcal mol⁻¹.¹² The kinetic parameters used in the previous reaction mechanisms are believed to cause significant uncertainties for isomerization reactions of biodiesels, even without showing rate constants in this section.

On the potential energy surfaces, the C–H β -fissions of MD radicals are generally characterized by high energy barriers and therefore will not be included in the following discussions. Consequently, the β -scission reaction hereinafter refers to the

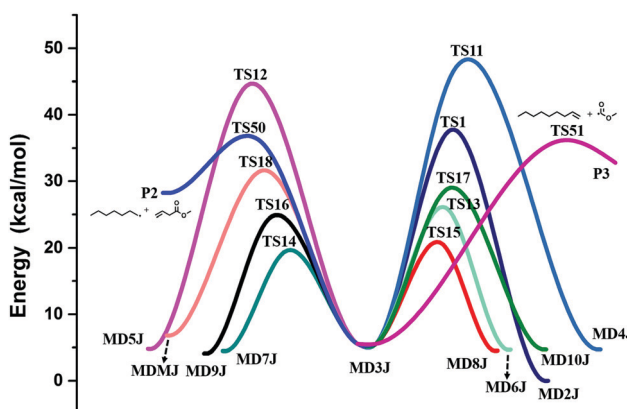


Fig. 2 Potential energy surface for the isomerization and β -scission reactions of MD3J at the ONIOM [QCISD(T)/CBS:DFT]//M06-2X/6-311++G(d,p) level.

Table 1 Energy barriers of β -scission reactions for MD radicals^a

Reactions	<i>E</i>	Ref.	Deviation
(MD2J)	31.6	33.0 ^b , 31.2 ^d	1.4 ^b , 0.4 ^d
(MD3J)	30.0	27.8 ^d	2.2 ^d
(MD3J)	30.6	33.5 ^b	2.9 ^b
(MD4J)	30.0	28.7 ^d	1.3 ^d
(MD4J)	25.0	26.5 ^b	1.5 ^b
(MD5J)	29.7	29.6 ^c	0.1 ^c
(MD5J)	30.6	30.1 ^c	0.5 ^c
(MD6J)	30.0	29.6 ^c	0.4 ^c
(MD6J)	29.9	29.6 ^c	0.3 ^c
(MD7J)	29.7	28.9 ^c	0.8 ^c
(MD7J)	30.2	30.1 ^c	0.1 ^c
(MD8J)	30.6	29.6 ^c	1.0 ^c
(MD8J)	29.9	29.9 ^c	0.0 ^c
(MD9J)	29.8	29.6 ^c	0.2 ^c
(MD10J)	30.0	29.4 ^c	0.6 ^c
(MDMJ)	33.2	33.9 ^b , 31.9 ^d	0.7 ^b , 1.3 ^d

^a Unit of *E* is kcal mol⁻¹. Notations *b*, *c*, and *d* represent available data of MB, *n*-decane and MD radicals from previous studies of Huynh *et al.*,²⁰ Zhao *et al.*,³⁴ and Glaude *et al.*,¹⁶ respectively.

C–C β -fissions of MD radicals. Energy barriers of the β -scission reactions ranging from 31.6 to 38.7 kcal mol⁻¹ are comparable with each other but generally higher than those of isomerization reactions. As the ester moieties in MD radicals have a vital influence on the β -scission reactions, the energy barriers and the available literature data for energetically favourable reaction channels are summarized in Table 1, for comparison. Available data of MB and *n*-decane from the previous studies are also listed in Table 1, for comparison.

For MD2J and MB2J, which are located in the α position from the ester moiety, and for MDMJ and MBMJ, which are alkoxyl radicals, comparable energy barriers of their dissociation reactions were observed, respectively, for the specific conjugation effect. Huynh *et al.*²⁰ investigated the isomerization and dissociation reactions of MB radicals at the BH&HLYP/cc-pVTZ level. The energy barriers of β -scissions of MB2J and MBMJ are 33.0 and 33.9 kcal mol⁻¹, which are higher than those of the corresponding MD radicals. Moreover, the dissociation

energy barriers of MD2J and MDMJ are in good agreement with the available literature data,¹⁶ with discrepancies being less than 1.3 kcal mol⁻¹. It is recognized that the effect of the ester functional group diminishes rapidly going away from the reaction center. Thus, the dissociation reactions of MD radicals located in positions farther than MD5J from the ester functionality show similar behavior with those of the corresponding *n*-decane radicals,³⁴ with deviations being less than 1.0 kcal mol⁻¹. For simplicity, only those energetically favorable reactions with transition states less than 37.0 kcal mol⁻¹ were implemented in the rate constant calculations in this work.

3.1.3 Discussion on entropies of MD radicals. To facilitate the discussion on rate constants in the following section, the entropies of MD radicals will be briefly discussed here. The pre-exponential factor (aka A-factor) in the rate coefficient expressions of TST is thermodynamically related to the entropy change ($\Delta S^\ddagger = S^\ddagger - S_R$) from the reactants to the transitions state. A tight transition state commonly has a smaller entropy

than a loose transition state. The ΔS^\ddagger at 298.15 K (denoted by ΔS^\ddagger for simplicity hereinafter without confusion) for isomerization and dissociation reactions for MD radicals is listed in Table S3 in the ESI,[†] where the corresponding reactions for MB radicals are listed for comparison.

For a transition state without the ester functionality in the transition state ring, an example is shown in Fig. S1 in the ESI.[†] The ΔS^\ddagger of the reactions from MD2J to MD3J, MD4J, MD5J, MD6J, MD7J, MD8J, MD9J and MD10J is -2.6 cal mol^{-1} , -5.1 cal mol^{-1} , -7.0 cal mol^{-1} , $-11.3\text{ cal mol}^{-1}$, $-12.9\text{ cal mol}^{-1}$, $-14.8\text{ cal mol}^{-1}$, $-17.4\text{ cal mol}^{-1}$ and $-16.3\text{ cal mol}^{-1}$, respectively, where ΔS^\ddagger decreases with increasing transition state ring size. The ΔS^\ddagger of the isomerization reaction from MD2J to MD10J is $-16.3\text{ cal mol}^{-1}$ and higher than $-17.4\text{ cal mol}^{-1}$ of the reaction from MD2J to MD9J. This is caused by the different electronic interactions of MD10J, where the radical is located at the terminal site. Compared with similar reactions in the MB system, the ΔS^\ddagger for the MD reactions is higher due to the longer aliphatic chain of the MD radicals.

For a transition state with the ester functionality in the transition state ring, an example is shown in Fig. S2 in the ESI.[†] The ΔS^\ddagger of the reactions from MD2J, MD3J, MD4J, MD5J, MD6J, MD7J, MD8J, MD9J and MD10J to MDMJ is -4.1 cal mol^{-1} , -6.1 cal mol^{-1} , $-10.5\text{ cal mol}^{-1}$, $-13.8\text{ cal mol}^{-1}$, $-15.4\text{ cal mol}^{-1}$, $-18.5\text{ cal mol}^{-1}$, $-22.4\text{ cal mol}^{-1}$, $-22.8\text{ cal mol}^{-1}$ and $-18.5\text{ cal mol}^{-1}$, respectively. The ΔS^\ddagger of the reaction from MD10J to MDMJ is $-18.5\text{ cal mol}^{-1}$ and higher than $-22.8\text{ cal mol}^{-1}$ of the reaction from MD9J to MDMJ, which is also attributable to the different electronic interactions of MD10J, where the radical is located at the terminal site. The comparison shows that the ΔS^\ddagger for the MD reactions is lower than those for the similar MB reactions, again because of the longer aliphatic chain of the MD radicals.

In addition, the ΔS^\ddagger in the β -scission reactions of other MD radicals is higher in comparison with the MB radicals. The exceptional case is that the ΔS^\ddagger of -2.9 cal mol^{-1} in the β -scission reaction of MD2J forming P1 is lower by 5.1 cal mol^{-1} than 2.2 cal mol^{-1} of the corresponding β -scission reaction of MB2J due to the strengthened conjugation effect caused by the longer aliphatic chain of the MD radicals.

3.2 High-pressure rate constants

3.2.1 Effects of ester functionality. Because the kinetic parameters of large methyl esters were mostly obtained by analogy to corresponding alkanes in previous studies,¹⁶ the comparison between them and the present calculations will be discussed first. As described above, the radical located in the α -site in terms of the ester functionality, such as MD2J, and the alkoxy radical, such as MDMJ, are representative radicals. Scarce available kinetic parameters of MD make the direct comparison unfeasible to conduct. Thus, the reactions involving these representative radicals, such as MD2J and MB2J, and MDMJ and MBMJ, were chosen respectively to show the difference between their isomerization reactions MD2J \rightarrow MDMJ and MB2J \rightarrow MBMJ, and that between their β -scission reactions MD2J \rightarrow P1 and MB2J \rightarrow P. The isomerization reactions MDMJ \rightarrow MD2J and

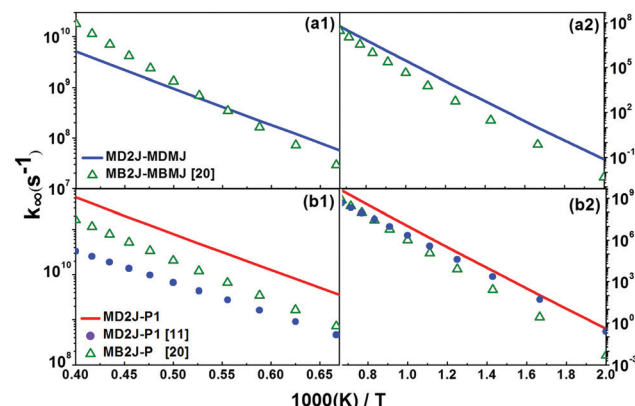


Fig. 4 High-pressure limit rate coefficients for the representative (a) isomerization and (b) dissociation reactions of MD2J. Rate coefficients of relevant reactions for MD¹¹ and MB²⁰ are shown for comparison.

MBMJ \rightarrow MB2J, and the β -scission reactions MDMJ \rightarrow P1 and MBMJ \rightarrow P are also shown for comparison.

Fig. 4 shows the high-pressure limit rate coefficients for the representative (a) isomerization and (b) dissociation reactions of MD2J. Relevant kinetic data of some isomerization and β -scission reactions for MB radicals by Huynh *et al.*²⁰ and for MD radicals by Herbinet *et al.*¹¹ are also shown for comparison. The temperature range considered in this work was split into two temperature regimes to facilitate the comparison. It can be seen that the rate constants of MD2J \rightarrow MDMJ are close to those of MB2J \rightarrow MBMJ only in a narrow temperature range around 2000 K. The one-order-of-magnitude difference of rate constants between MD2J \rightarrow MDMJ and MB2J \rightarrow MBMJ is observed at temperatures less than 800 K, due to their energy differences. At low temperatures, the rate constants of MB2J \rightarrow P are lower than those of MD2J \rightarrow P1, whereas the rate constants of MD2J \rightarrow P1 obtained by Glaude *et al.*¹⁶ agree well with the present results. As already shown in Table 1, the energy barriers of MD2J \rightarrow P1 obtained in this work and by Glaude *et al.*¹⁶ are 31.6 and 31.2, respectively.

Fig. 5 shows the high-pressure limit rate coefficients for the representative (a) isomerization and (b) dissociation reactions of MDMJ. At temperatures below 700 K, the rate constants of MDMJ \rightarrow MD2J (with the energy barrier of $26.3\text{ kcal mol}^{-1}$) are significantly higher than that of MBMJ \rightarrow MB2J (with the energy barrier of about 35 kcal mol^{-1}) obtained by Huynh *et al.*²⁰ and that of MDMJ \rightarrow MD2J (with the energy barrier of $34.6\text{ kcal mol}^{-1}$) obtained by Herbinet *et al.*¹¹ derived from smaller etsers. For the β -scission reaction, the rate constants of MDMJ \rightarrow P16 (with the energy barrier $33.2\text{ kcal mol}^{-1}$) are close to those of MBMJ \rightarrow P (with an energy barrier $33.9\text{ kcal mol}^{-1}$) at low temperatures, but they differ from each other by a factor of 50 at the temperature of 2500 K. As discussed above, the large difference of the β -scission reactions between MBMJ and MDMJ is caused by their entropy difference. The entropy change for MDMJ \rightarrow P16 is -5.8 cal mol^{-1} and lower than that for MBMJ by 4.7 cal mol^{-1} , which is attributable to the large difference of their rate constants at high temperatures.

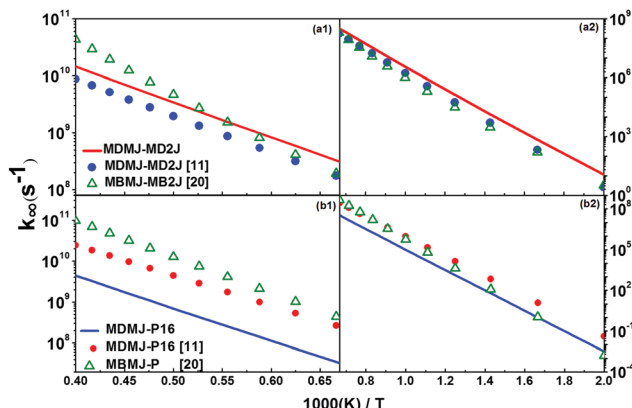


Fig. 5 High-pressure limit rate coefficients for the representative (a) isomerization and (b) dissociation reactions of MDMJ radical. Rate coefficients of relevant reactions for MD 11 and MB20 are shown for comparison.

Additionally, the rate constant of $\text{MDMJ} \rightarrow \text{P16}$ obtained by Herbinet *et al.*¹¹ is higher than the present calculation results by one order of magnitude, probably because they underestimated the energy barriers obtained by analogy to alkanes.

3.2.2 Comparison with alkyls. The ester moiety has significant effects on the reactivity of adjacent groups by strong conjugation, and its influence is reduced dramatically as the aliphatic chain increases. Thus, it is feasible to construct biodiesel kinetic mechanisms based on the rate constants of corresponding alkanes. Fig. 6(a) is the illustration of the difference for the isomerization reactions of (a) $\text{MD10J} \rightarrow \text{MD7J}$ and (b) $\text{MDMJ} \rightarrow \text{MD3J}$ between the calculated and estimated rate coefficients at the high-pressure limit.^{11,20} In the present system, MD10J with its radical position at the terminal site of the aliphatic chain is most similar to an alkyl radical. The isomerization reaction of $\text{MD10J} \rightarrow \text{MD7J}$ was thereby used to illustrate the kinetic difference as a result of using the analogous method. It can be seen that the rate constants for $\text{MD10J} \rightarrow \text{MD7J}$ obtained by analogy to alkanes are higher than the present results and the difference between them decreases as temperature increases.

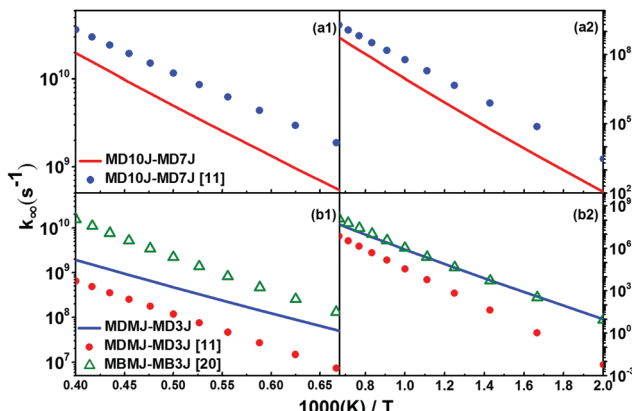


Fig. 6 Illustration of the difference for the isomerization reactions of (a) $\text{MD10J} \rightarrow \text{MD7J}$ and (b) $\text{MDMJ} \rightarrow \text{MD3J}$ between the calculated and estimated rate coefficients at the high pressure limit.^{11,20}

At low and intermediate temperatures, isomerization reactions play an important role, and using the kinetic parameters of isomerization reactions by analogy to alkanes may cause different low-temperature behaviors.

Although MDMJ is a typical radical of methyl ester, the rate constant of the isomerization from MDMJ to MD3J was approximated to be close to that of alkane radicals in MD combustion modeling.¹¹ Thus, the isomerization reaction of $\text{MDMJ} \rightarrow \text{MD3J}$ was chosen to examine the difference caused by the approximation method. As illustrated in Fig. 6(b), the difference of the rate constants for $\text{MDMJ} \rightarrow \text{MD3J}$ between the MD combustion modeling and the present results can be as large as three orders of magnitude at 500 K and decreases as temperature increases. This indicates that it is unreliable in producing rate constants by analogy to *n*-decane for these isomerization reactions. As discussed above in Section 3.1, the significantly different energy barriers of isomerization reactions between the alkane and methyl ester systems are attributable to the huge difference. Consequently, the approximation method used to estimate the rate constants is questionable, especially for the radicals surrounded by the ester functionality.

The comparison between the present predictions of the rate constants of β -scission reactions of MD4J and MD10J and the available literature data^{11,20} is shown in Fig. 7. It can be seen that at intermediate and high temperatures, the present predictions of the β -scission reactions of $\text{MD4J} \rightarrow \text{P5}$ are close to those of MB4J reported by Huynh *et al.*²⁰ and those of MD4J of Herbinet *et al.*¹¹ For the β -scission reaction of $\text{MD10J} \rightarrow \text{P15}$ at low temperatures, the calculated rate constants are close to those derived from alkanes by using the approximation methods. Their discrepancy becomes increasingly large with increasing temperature.

Based on the above discussion, it is reasonable to predict the rate constant of $\text{MDMJ} \rightarrow \text{MD2J}$ and its reverse reaction by analogy to the biodiesel surrogate MB,²⁰ but the rate constants of other isomerization reactions in the MD system could bring huge uncertainties if they are derived from alkanes and MB.¹¹ Moreover, the rate constants of β -scission reactions are

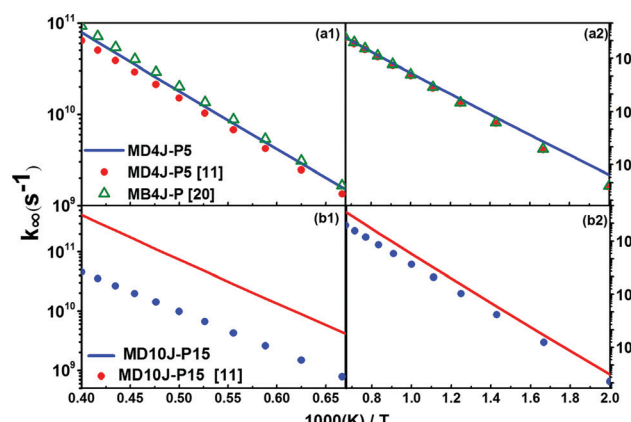


Fig. 7 Illustration of differences for the isomerization reactions of (a) $\text{MD4J} \rightarrow \text{P5}$ and (b) $\text{MD10J} \rightarrow \text{P15}$ between the calculated and estimated rate coefficients at the high pressure limit.^{11,20}

distinguished at low temperatures due to different energy barriers and at high temperatures due to different entropies. This can explain why the rate constants of the β -scission reactions in the MD system obtained by analogy to alkanes and MB are sometimes reasonable since these β -scission reactions have comparable energy barriers.

3.3 Pressure-dependent rate constants

3.3.1 Pressure-dependence of the reactions of MD2J. The pressure-dependent rate constants for three representative reactions of MD2J are illustrated in Fig. 8, where the pressure-dependent rate plots at intermediate and high temperatures have been zoomed in to manifest their difference. It was found that there is no significant pressure dependence in the lower temperature range of 500–900 K, as we anticipated. At higher temperatures, the rate constants can be different from their high-pressure limits by several times. The temperature threshold for considering the pressure dependence increases with increasing pressure.

It can be seen that the pressure-dependent rate plots end at certain temperatures due to the “well merging” phenomena in the reaction system.³³ At sufficiently high temperatures, it is common for some of the radical isomers (*i.e.* potential wells) to rapidly equilibrate with each other or with bimolecular products.

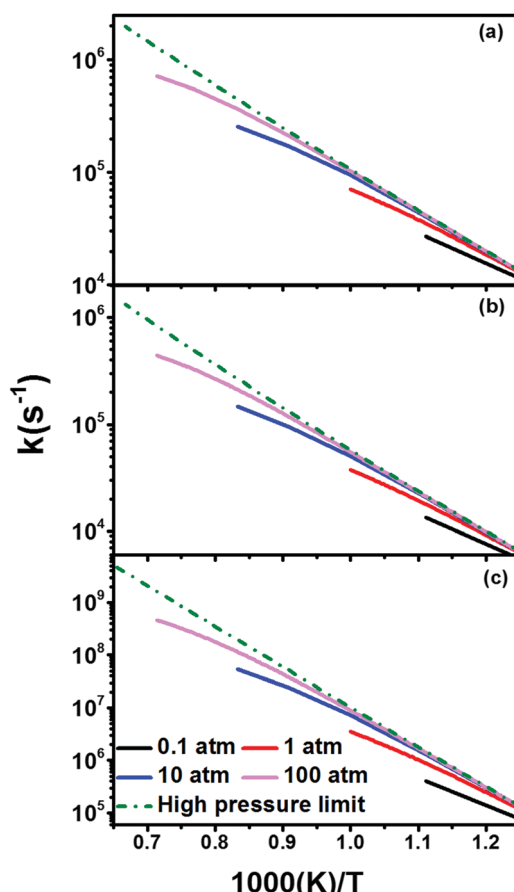


Fig. 8 The temperature and pressure-dependent rate coefficients for kinetically favourable reactions of MD2J. (a) MD2J–MD6J, (b) MD2J–MD7J, and (c) MD2J–P1.

The phenomena of well merging occur when the rate of isomerization (or dissociation) reaction from one well to another well (or bimolecular products) becomes comparable to the rate of its internal energy relaxation due to the molecular collision. Consequently, beyond the temperature at which the well merging occurs, the merged wells become chemically indistinguishable and should be considered as a “combined” well, and the total number of wells in the PES is accordingly reduced by one. In the present work, the well-reduction based on the multi-well master equation analysis will not be discussed in detail, and a recently developed method that automates this reduction process has been incorporated into the MESS computer code.

Regarding the pressure dependence of the rate constants at all pressures considered in this work, the branching ratios of reactions from MD2J at 0.1 atm, 1 atm, 10 atm and 100 atm are shown in Fig. 9. Although the branching ratios of the main isomerization reactions decline rapidly with increasing temperature, they are the predominant consumption channels at low temperatures. In contrast, the branching ratio of the β -scission (MD2J \rightarrow P1) undergoes a rapid growth and reaches approximate equilibrium at sufficiently high temperatures. At a temperature from about 600 K to 800 K, the isomerization and dissociation reactions are comparably important. Therefore, the distribution of MD radicals depends on not only the initial steps but also the isomerization reactions, which may affect the autoignition properties of MD.

3.3.2 Pressure-dependence of the reactions of MD3J. The pressure-dependent rate coefficients for kinetically favourable reactions from MD3J are shown in Fig. 10. The trends of these rate coefficients are overall similar to that of MD2J. For isomerization reactions from MD3J, there is no significant pressure dependence at temperatures below 1000 K, and moderate pressure dependence can be seen in evidence at temperatures above 1100 K. The well merging temperature for the isomerization reaction from MD3J to MD7J increases from 1000 K at 0.1 atm to 2000 K at 10 atm.

The branching ratios of the reactions for MD3J at 0.1 atm, 1 atm, 10 atm, and 100 atm are shown in Fig. 11. The rate

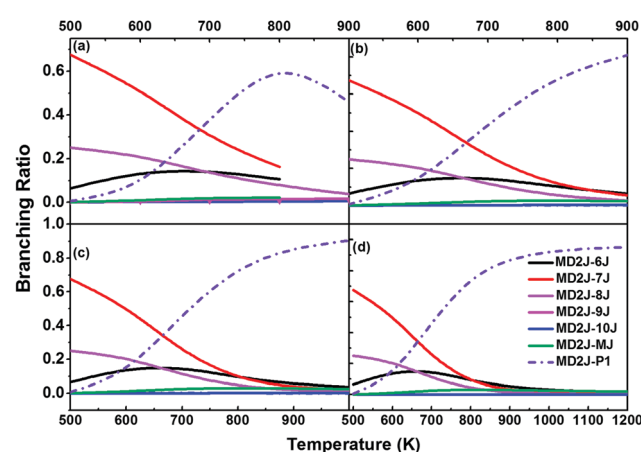


Fig. 9 Temperature-dependent branching ratios for main reactions of MD2J at (a) 0.1 atm, (b) 1 atm, (c) 10 atm, and (d) 100 atm.

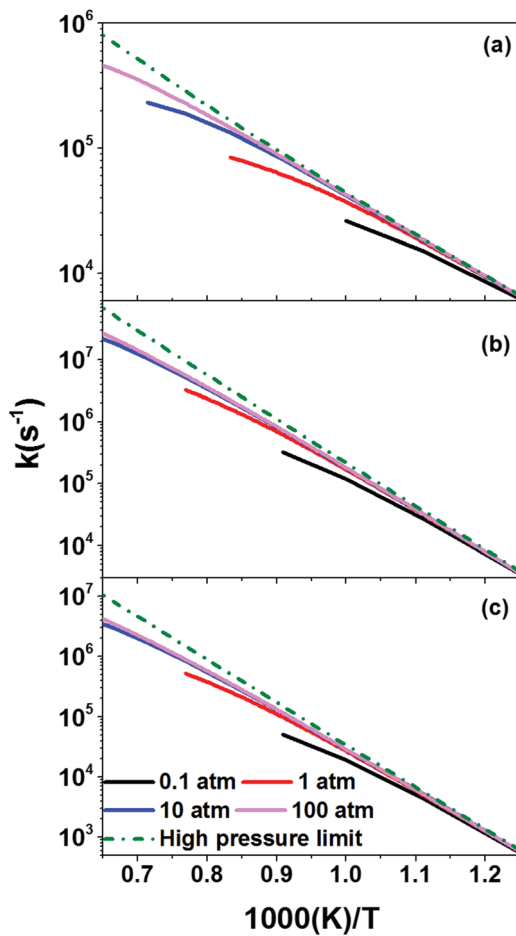


Fig. 10 The temperature and pressure-dependent rate coefficients for kinetically favorable reactions of MD3J. (a) MD3J–MD7J, (b) MD3J–P2, and (c) MD3J–P3.

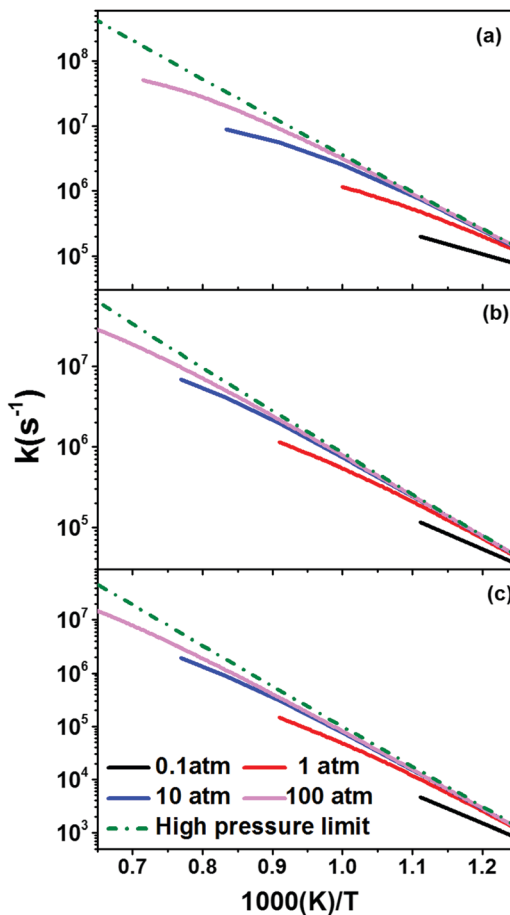


Fig. 12 The temperature and pressure-dependent rate coefficients for kinetically favorable reactions of MDMJ. (a) MDMJ–MD2J, (b) MDMJ–MD3J, and (c) MDMJ–P16.

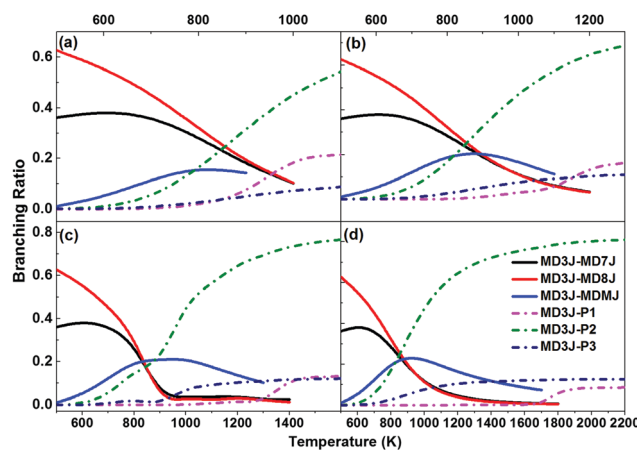


Fig. 11 Temperature-dependent branching ratios for main reactions of MD3J at (a) 0.1 atm, (b) 1 atm, (c) 10 atm, and (d) 100 atm.

constants of P2 formation are slightly higher than those of P3 formation at low temperatures due to its slightly lower energy barrier. At high temperatures, the P2 formation becomes more competitive in the consumption of MD3J. As pressure increases,

the rate coefficients of the dissociation reactions increase to approach their high-pressure limits.

3.3.3 Pressure-dependence of the reactions of MDMJ.

Fig. 12 shows the temperature- and pressure-dependent rate coefficients of kinetically favorable reactions of MDMJ. The well merging temperature is about 900 K at 0.1 atm and increases to 2400 K at 100 atm. No well merging was observed for MDMJ → MD2J and MDMJ → MD3J at 100 atm below 1400 K. As discussed above, the pressure dependence for the rate coefficients at these pressures is moderate, since the well is difficult to stabilize at higher temperatures. The obvious pressure fall-off at 1 atm starts at a temperature of about 900 K by a factor of 3. The significant fall-off indicates that most of the entrance channel flux returns to the MDMJ radicals at high temperatures.

The temperature-dependent branching ratios for the reactions of MDMJ at 0.1 atm, 1 atm, 10 atm and 100 atm are shown in Fig. 13. For temperatures from 500 K to 1400 K, the dominant reaction channels are the isomerization reactions from MDMJ with the overall branching ratio being about 60%. The branching ratio of the isomerization from MDMJ to MD2J increases with temperature, reaches the maximum at 1000 K, and then declines with further increasing temperature. Eventually, this isomerization reaction vanishes at 1400 K due to the

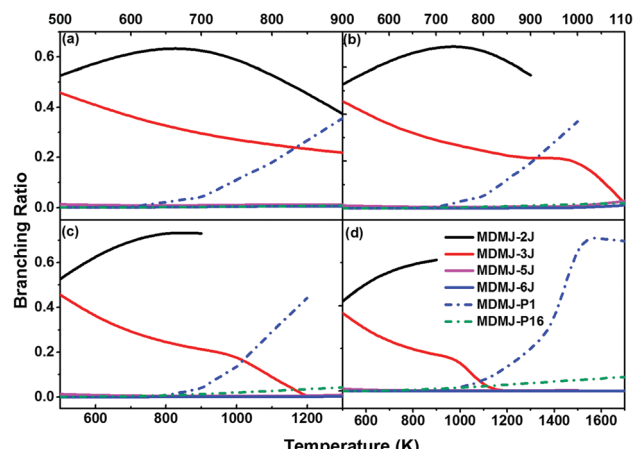


Fig. 13 Temperature-dependent branching ratios for main reactions of MDMJ at (a) 0.1 atm, (b) 1 atm, (c) 10 atm, and (d) 100 atm.

well merging. As can be seen in the PES, there is no direct connection between P1 and MDMJ. As temperature increases, the branching ratios for the P1 formation increase slowly at first and then show a rapid growth at temperatures above 1300 K. The branching ratios of the β -scission reaction from MDMJ to P16 remain low at low temperatures and then grow up slowly at temperatures above 1400 K. It can be concluded that 90% of MDMJ radicals are isomerized and decomposed to P1 and P16 at high temperatures. Furthermore, it is also shown that the branching ratios for the isomerization reaction to MD3J decline with increasing temperature, while those for the reaction to MD2J become more competitive as temperature increases.

The calculated high-pressure limit rate constants of key reactions fitted in the Arrhenius form are given in Table 2. The pressure-dependent rate coefficients of reactions for all the MD radicals, tabulated for different pressures and in the two-Arrhenius forms, are given in Table S5 in the ESI.[†]

Table 2 Rate constants of key reactions for MD radicals at the high pressure limit^a

Reactions	<i>A</i>	<i>n</i>	<i>E</i> ^a	Reactions	<i>A</i>	<i>n</i>	<i>E</i> ^a
MD2J \rightarrow 6J	3.8×10^3	1.5	13.9	MDMJ \rightarrow 2J	3.7×10^9	0.8	25.1
MD2J \rightarrow 7J	7.8	2.6	13.2	MDMJ \rightarrow 3J	3.1×10^5	1.7	20.7
MD3J \rightarrow 7J	1.1×10^2	1.8	12.3	MD2J \rightarrow P1	3.1×10^{11}	0.9	33.1
MD3J \rightarrow 8J	1.2×10^3	1.3	11.8	MD3J \rightarrow P2	1.5×10^9	0.9	30.4
MD4J \rightarrow 8J	9.1×10^4	1.3	13.9	MD3J \rightarrow P3	2.7×10^8	0.9	30.3
MD4J \rightarrow 9J	15.9	2.1	10.2	MD4J \rightarrow P4	6.0×10^{13}	0.1	31.1
MD5J \rightarrow 9J	4.2×10^3	1.7	12.8	MD4J \rightarrow P5	2.0×10^{13}	0.8	25.9
MD5J \rightarrow 10J	41.4	2.1	12.3	MD5J \rightarrow P6	3.4×10^{11}	0.5	30.9
MD6J \rightarrow 9J	15.1	2.8	20.0	MD5J \rightarrow P7	1.3×10^{10}	0.9	29.9
MD6J \rightarrow 10J	11.3	2.5	13.5	MD6J \rightarrow P8	1.4×10^8	1.3	29.5
MD7J \rightarrow 2J	5.0×10^{-2}	2.7	9.2	MD6J \rightarrow P9	8.3×10^9	0.9	30.3
MD7J \rightarrow 3J	6.6	2.2	12.8	MD7J \rightarrow P10	2.4×10^9	0.9	29.4
MD8J \rightarrow 3J	59.4	1.8	12.3	MD7J \rightarrow P11	2.4×10^8	1.3	29.4
MD8J \rightarrow 4J	1.2×10^3	1.7	13.9	MD8J \rightarrow P12	5.7×10^9	1.0	32.2
MD9J \rightarrow 4J	0.5	2.5	9.7	MD8J \rightarrow P13	2.7×10^{10}	0.5	30.7
MD9J \rightarrow 5J	1.6×10^2	2.0	12.0	MD9J \rightarrow P14	1.1×10^8	1.3	28.3
MD10J \rightarrow 5J	1.4×10^2	2.1	10.7	MD10J \rightarrow P15	8.4×10^{10}	1.0	30.2
MD10J \rightarrow 6J	4.1×10^4	1.7	12.4	MDMJ \rightarrow P16	3.6×10^9	0.9	32.7

^a Units of *A* and *E*_a are s⁻¹ and kcal mol⁻¹, respectively. *k*(*T*) = *AT*^{*n*} exp(-*E*_a/RT).

4. Conclusions

In the present theoretical study, the rate constants of the isomerization and dissociation reactions for methyl decanoate radicals were calculated by using the transition state theory. A high-level two-layer ONIOM method was employed to predict single point energies of all the reactions considered. Phenomenological rate constants of the isomerization and dissociation reactions of methyl decanoate radicals were obtained by the RRKM/ME theory. In addition to providing accurate rate constants for the kinetic modeling of MD combustion, the explored reactivity–structure relationships for the isomerization and dissociation reactions of MD radicals can be applied to realistic biodiesel combustion chemistry. At intermediate temperatures, intense competition between isomerization and dissociation reactions, determining the distribution of MD radicals, is of great significance to autoignition. At temperatures higher than 1100 K, the chemical kinetics of MD radicals is well described by the dissociation via β -scissions. Moreover, the significant pressure dependence of the rate constants was observed for the isomerization and dissociation reactions of MD radicals.

Compared with the available literature data of MB, *n*-decane, and MD, great discrepancies between MB and MD have been found for the reactions specific to methyl esters. The present results suggest that kinetic parameters used in MD modeling by analogy to corresponding alkanes have significant errors for isomerization reactions, whereas they are approximately suitable for simulating the β -scission reactions of MD because of their comparable energy barriers. Theoretical studies focusing on the isomerization and dissociation reactions of MD radicals provide deep insight into their combustion chemistry, which is also beneficial to improve the chemical kinetic modeling of biodiesel oxidation.

Conflicts of interest

There are no conflicts to declare.

Acknowledgements

The work at Hong Kong Polytechnic University was supported by NSFC (No. 91641105), and partly by the university matching grant (4-BCE8). The work at the University of Science and Technology of China was supported by Natural Science Foundation of China (51676176, U1532137, 11575178 and 21373193), National Key Scientific Instruments and Equipment Development Program of China (2012YQ22011305), and Fundamental Research Funds for the Central Universities (WK2320000038).

References

- 1 A. K. Agarwal, *Prog. Energy Combust. Sci.*, 2007, **33**, 233–271.
- 2 K. Kohse-Hoinghaus, P. Osswald, T. A. Cool, T. Kasper, N. Hansen, F. Qi, C. K. Westbrook and P. R. Westmoreland, *Angew. Chem., Int. Ed. Engl.*, 2010, **49**, 3572–3597.
- 3 J. Y. W. Lai, K. C. Lin and A. Violi, *Prog. Energy Combust. Sci.*, 2011, **37**, 1–14.

- 4 L. Meher, D. V. Sagar and S. Naik, *Renewable Sustainable Energy Rev.*, 2006, **10**, 248–268.
- 5 G. Knothe, *Prog. Energy Combust. Sci.*, 2010, **36**, 364–373.
- 6 C. V. Naik, C. K. Westbrook, O. Herbinet, W. J. Pitz and M. Mehl, *Proc. Combust. Inst.*, 2011, **33**, 383–389.
- 7 C. K. Westbrook, C. V. Naik, O. Herbinet, W. J. Pitz, M. Mehl, S. M. Sarathy and H. J. Curran, *Combust. Flame*, 2011, **158**, 742–755.
- 8 S. Bax, M. H. Hakka, P.-A. Glaude, O. Herbinet and F. Battin-Leclerc, *Combust. Flame*, 2010, **157**, 1220–1229.
- 9 Q. Meng, X. Zhao, L. Zhang, P. Zhang and L. Sheng, *Combust. Flame*, 2018, **196**, 45–53.
- 10 G. Knothe, S. C. Cermak and R. L. Evangelista, *Energy Fuels*, 2009, **23**, 1743–1747.
- 11 O. Herbinet, W. J. Pitz and C. K. Westbrook, *Combust. Flame*, 2008, **154**, 507–528.
- 12 H. J. Curran, P. Gaffuri, W. J. Pitz and C. K. Westbrook, *Combust. Flame*, 1998, **114**, 149–177.
- 13 H. J. Curran, P. Gaffuri, W. J. Pitz and C. K. Westbrook, *Combust. Flame*, 2002, **129**, 253–280.
- 14 E. M. Fisher, W. J. Pitz, H. J. Curran and C. K. Westbrook, *Proc. Combust. Inst.*, 2000, **28**, 1579–1586.
- 15 O. Herbinet, W. J. Pitz and C. K. Westbrook, *Combust. Flame*, 2010, **157**, 893–908.
- 16 P. A. Glaude, O. Herbinet, S. Bax, J. Biet, V. Warth and F. Battin-Leclerc, *Combust. Flame*, 2010, **157**, 2035–2050.
- 17 P. Diévert, S. H. Won, J. Gong, S. Dooley and Y. Ju, *Proc. Combust. Inst.*, 2013, **34**, 821–829.
- 18 E. Papajak and D. G. Truhlar, *J. Phys. Chem.*, 2012, **137**, 064110.
- 19 J. Zádor, C. A. Taatjes and R. X. Fernandes, *Prog. Energy Combust. Sci.*, 2011, **37**, 371–421.
- 20 L. K. Huynh and A. Violi, *J. Org. Chem.*, 2008, **73**, 94–101.
- 21 L. Zhang, Q. Chen and P. Zhang, *Proc. Combust. Inst.*, 2015, **35**, 481–489.
- 22 X. Zhou, Y. Zhai, L. Ye and L. Zhang, *Sustainable Energy Fuels*, 2018, **2**, 392–402.
- 23 S. P. Pyl, C. M. Schietekat, K. M. Van Geem, M.-F. Reyniers, J. Vercammen, J. Beens and G. B. Marin, *J. Chromatogr. A*, 2011, **1218**, 3217–3223.
- 24 L. Zhang and P. Zhang, *Phys. Chem. Chem. Phys.*, 2015, **17**, 200–208.
- 25 L. Zhang, Q. Meng, Y. Chi and P. Zhang, *J. Phys. Chem. A*, 2018, **122**, 4882–4893.
- 26 M. Frisch, G. Trucks, H. B. Schlegel, G. Scuseria, M. Robb, J. Cheeseman, G. Scalmani, V. Barone, B. Mennucci and G. Petersson, *Gaussian 09*, Gaussian, Inc., Wallingford, CT, 2009.
- 27 C. Eckart, *Phys. Rev.*, 1930, **35**, 1303.
- 28 P. Zhang, S. J. Klippenstein and C. K. Law, *J. Phys. Chem. A*, 2013, **117**, 1890–1906.
- 29 P. Diévert, S. H. Won, S. Dooley, F. L. Dryer and Y. Ju, *Combust. Flame*, 2012, **159**, 1793–1805.
- 30 H. Hippler, J. Troe and H. Wendelken, *J. Chem. Phys.*, 1983, **78**, 6709–6717.
- 31 S. J. Klippenstein and J. A. Miller, *J. Phys. Chem. A*, 2002, **106**, 9267–9277.
- 32 B. Sirjean, E. Dames, H. Wang and W. Tsang, *J. Phys. Chem. A*, 2012, **116**, 319–332.
- 33 Y. Georgievskii, J. A. Miller, M. P. Burke and S. J. Klippenstein, *J. Phys. Chem. A*, 2013, **117**, 12146–12154.
- 34 L. Zhao, T. Yang, R. I. Kaiser, T. P. Troy, M. Ahmed, D. Belisario-Lara, J. M. Ribeiro and A. M. Mebel, *J. Phys. Chem. A*, 2017, **121**, 1261–1280.